Biophysical Chemistry 151 (2010) 71–80

Contents lists available at ScienceDirect

Biophysical Chemistry

journal homepage: http://www.elsevier.com/locate/biophyschem

A model for processive movement of single-headed myosin-IX

Ping Xie *

Key Laboratory of Soft Matter Physics and Beijing National Laboratory for Condensed Matter Physics, Institute of Physics, Chinese Academy of Sciences, Beijing 100190, China

ARTICLE INFO

Article history:
Received 16 April 2010
Received in revised form 14 May 2010
Accepted 14 May 2010
Available online 21 May 2010

Keywords:
Molecular motor
Processivity
Mechanochemical coupling
Brownian motion

ABSTRACT

It is puzzling that in spite of its single-headed structure, myosin-IX can move processively along actin. Here, based on the experimental evidence that the strong binding of myosin to actin in rigor state induces structural changes to several local actin monomers, a Brownian ratchet model is proposed to describe this processive movement. In the model, the actin plays an active role in the motility of single-headed myosin, in contrast to the common belief that the actin acts only as a passive track for the motility of the myosin. The unidirectional movement is due to both the asymmetric periodic potential of the myosin interacting with actin and the forward Stokes force induced by the relative rotation of the neck domain to the motor domain, while the processivity is determined by the binding affinity of the myosin for actin in ATP state. This gives a good explanation to the high processivity of myosin-IX, which results from its high binding affinity for actin in ATP state due to the presence of unique loop 2 insertion or N-terminal extension. The experimental results on the motility of myosin-IX such as the step size, large forward/backward stepping ratio, run length, stall force, etc, are explained well.

1. Introduction

Myosin-IX is demonstrated to be able to move processively along actin using the chemical energy liberated by ATP hydrolysis [1–4]. In contrast to other actin-based processive motors such as myosin-V that has a two-headed structure [5,6], myosin-IX has only one head. For the dimers, it has been demonstrated that the motors move processively in a hand-over-hand manner along actin [7] and the processivity is supposed to ensure that one head is bound strongly to actin when the other head is stepping forward [6–15]. What is puzzling to us, however, is how the monomers can also make processive movement.

In the literature, the prevailing model for the unidirectional movement of the monomeric molecular motors such as the single-headed kinesin is the fluctuating thermal ratchet model [16–18]. In this model, the monomer is treated as a Brownian particle that moves in an asymmetric periodic potential with a deep depth. Nucleotide transition in the motor changes something about the motor, which sees a new potential but with a very shallow depth. This fluctuation of the potential breaks balance and thus unidirectional movement becomes possible. The remaining issue for this model is why the monomer cannot detach from its track during the weak-actin-binding (or simply called weak binding) period with the potential of a very shallow depth. To explain both the high processivity and the unidirectional movement for single-headed myosin-IX, Ikebe and his coworkers recently proposed an inchworm-like model [4,19]. In this model, it was assumed that during the weak-binding period (e.g., in ATP and ADP.Pi states) myosin-IX repeatedly attaches and detaches from actin which is anchored by loop 2. When myosin-IX is attached to the forward binding site the strain sensor triggers Pi release, converting the weak-binding state to a strong-binding one, and then loop 2 dissociates from actin and returns to its original length. Based on the similar spirit, Ikebe and his coworkers proposed a model to explain their observed directional motion of a large bead tethered to an actin filament via a single-headed myosin-VI molecule [20]. During the rigor binding state of the myosin-VI head, when the bead diffuses towards the minus end of the actin a sufficient distance, the myosin head is pulled in the minus-end direction, accelerating ATP binding. After dissociating from the actin, the rapid Brownian motion of the myosin head causes it to preferentially land at the next actin target in the minus-end direction. Strong binding to the actin is accompanied by Pi release and then is followed by ADP release. Thus, during one ATPase cycle, the bead moves in the minus-end direction by one step.

In this work, we proposed a new Brownian ratchet model for the processive movement of single-headed myosin-IX molecular motor by incorporating the effect of the conformational changes in several local actin monomers induced by the strong binding of ADP/nucleotide-free myosin. One idea in the model is that, during the weak-binding period, besides the effect of the asymmetric periodic potential, the presence of a forward Stokes force resulting from the large conformational change can contribute further to the unidirectional movement, whereas during the strong-binding period, the motor remains fixed to the track regardless of any external forces such as the backward Stokes force and the thermal noise. Another idea is that the local interaction of myosin with actin immediately after ATP

* Tel.: +86 10 82649387; fax: +86 10 82640224.
E-mail address: pxie@aphy.iphy.ac.cn.

0301-4622/$ – see front matter © 2010 Elsevier B.V. All rights reserved.
doi:10.1016/j.bpc.2010.05.007

binding is much weaker than the potential elsewhere, which results from the conformational changes in several local actin monomers induced by the strong binding of the ADP/nucleotide-free myosin. The non-weak interaction between ATP–myosin-IX and unaffected actin monomers ensures a high processivity of the single-headed myosin-IX.

2. Model

Before the presentation of our model, we first present two hypotheses in the following two sections.

2.1. Interaction potential of myosin with actin

From the experimental evidence [21–25], it is known that the interaction between a myosin motor domain and actin depends on its nucleotide state. Generally, in ADP and nucleotide-free states, the motor domain has a strong interaction with actin. In ATP and ADP.Pi states, the motor domain has a weak interaction with actin. In detail, we describe the evolution of the interaction force between the motor domain and actin during one ATPase cycle as follows.

We start with the motor domain binding strongly to actin in ADP state, with their interaction potential being written as $V_s(x, y) = V_s^{(x)} \exp[-(y-y_0)/a]$ $(y \geq y_0)$, where $V_s^{(x)} \leq 0$ (with the maxima equal to zero) represents the periodic piecewise potential along actin (or along the longitudinal direction) and is schematically shown in Fig. 1a. The term $\exp[-(y-y_0)/a]$ denotes the potential change in the direction perpendicular to the actin (or in the vertical direction), with a characterizing the interaction distance, which corresponds approximately to the Debye length inside cell. Note that, due to the steric restriction of the actin, the position of the motor domain is confined to the region $y \geq y_0$. This potential in the vertical direction is similar to the Morse potential that describes the van der Waals interaction. The asymmetric potential $V_s^{(x)}$, with one side of $V_s^{(x)}$ in a period being steeper than the other (see Fig. 1a), is due to the asymmetric charge distributions on the interacting surfaces of both the actin monomer and the motor domain. The period of $V_s^{(x)}$, $d = 5.5$ nm, is equal to the distance between two successive binding sites (or monomers) on the actin and the asymmetry is characterized by a parameter $\alpha \equiv d_s/d$, where d_s is the length of the part of the period with steeper slope (see Fig. 1a). After ADP release, the nucleotide-free motor domain remains bound strongly to actin, with their interaction potential being still described by $V_s(x, y)$, as defined above.

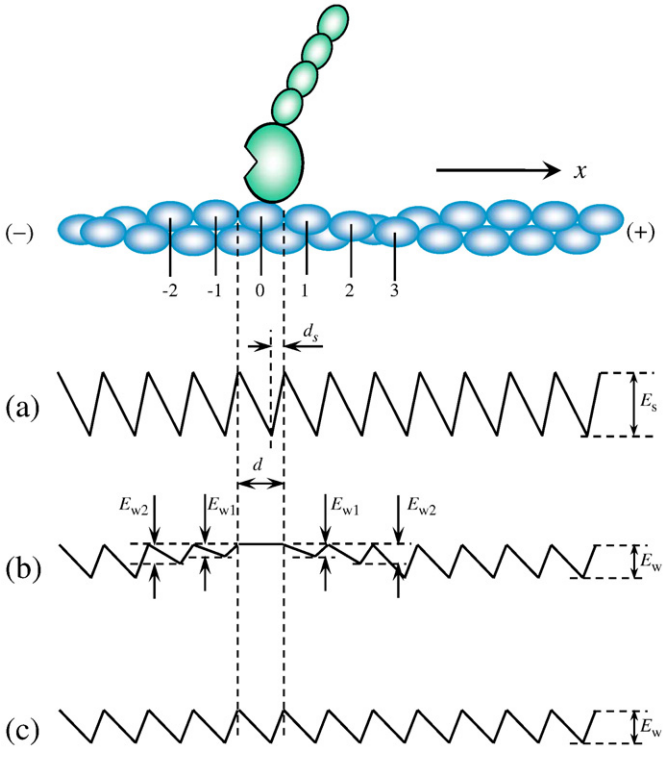

Fig. 1. Interaction potential of the myosin motor domain with actin in the x direction (along actin) during one ATPase cycle. (a) Strong interaction potential, $V_s^{(x)}(x)$, in ADP and nucleotide-free states. The potential depth E_s may be different for different nucleotide states and the binding affinity of rigor myosin to several local actin monomers may be different from other monomers. Here, for simplicity but without influence of our results, we draw the same binding affinity E_s for all actin monomers. (b) Weak interaction potential, $V_w^{(x)}(x)$, in ATP state immediately after ATP binding. (c) Weak interaction potential $V_w^{(x)}(x)$ in ATP or ADP.Pi state in a period of time t_r after ATP binding. The top figure shows the position of the myosin in rigor state binding strongly to actin monomer 0. See text for the detailed discussion on the evolution of potential $V_w^{(x)}$ (b and c) after ATP binding.

Immediately after ATP binding, the interaction potential becomes the one that can be written as $V_w(x, y) = V_w^{(x)} \exp[-(y-y_0)/a]$ $(y \geq y_0)$, with $V_w^{(x)} \leq 0$ (with the maxima equal to zero) being schematically shown in Fig. 1b. Note that the binding affinities of several local actin-binding sites for ATP–myosin near which the motor domain has just bound in ADP and/or nucleotide-free states become even weaker than other binding sites. After a period of time, t_r, the binding affinities of the several local actin-binding sites relax to the normal value and the potential $V_w^{(x)}$ becomes that shown schematically in Fig. 1c. After hydrolysis of ATP to ADP.Pi, the potential $V_w^{(x)}$ is still in the form of Fig. 1c. The explanation to the evolution of potential $V_w^{(x)}$ after ATP binding, as shown in Fig. 1b and c, is given as follows.

The ATP binding induces the conformational change in the actin-binding site of myosin motor domain, i.e., the conformational change from the closed to open clefts between the 50 kDa subdomains [23], which results in its weak interaction with actin. On the other hand, it has been acknowledged that the strong interaction with actin of the myosin in ADP and nucleotide-free states results in a structural change to the local actin monomer and such a change is propagated significantly beyond the actin monomer that is in contact with myosin [26]. As further evidenced by Prochniewicz et al. [27], this effect of myosin-induced conformational change of the single actin monomer can propagate to a group of four to five nearby monomers. It is thus expected that, after ATP-binding-induced detachment of the bound myosin, the conformations of the five local actin monomers (which are labeled as monomers 0, ± 1 and ± 2 in the top of Fig. 1) should still be different from others temporarily. On the other hand, the binding affinity of the actin monomer for myosin is dependent on the conformation of the actin monomer. Thus, we expect that the ATP–myosin-IX complex should either have a further weaker interaction or have a stronger interaction with the five local actin monomers than those with the unaffected actin monomers. Here it is reasonable to assume that the ATP–myosin-IX complex has a further weaker interaction with the five local actin monomers (noting that the stronger interaction of the ATP–myosin-IX complex with the five local actin monomers induces the non-unidirectional motion of the myosin along the actin). Moreover, it is taken for granted that the actin monomer (monomer 0) to which the motor domain in nucleotide-free state is binding has a largest conformational change and, as monomers (monomers ± 1 and ± 2) are far away from monomer 0, their conformational changes become smaller. Correspondingly, the binding affinity of ATP–myosin-IX complex for monomer 0 has the smallest value, the affinity for monomers ± 1 is larger than that for monomer 0, and the affinity for monomers ± 2 is larger than that for monomers ± 1, as shown in Fig. 1b. After a period of time t_r the elastic deformations of the five local binding sites (or monomers 0, ± 1 and ± 2) relax to their normal conformations and thus the interactions of the ATP–myosin with these binding sites of actin become the same as those with other unaffected binding sites, as shown in Fig. 1c.

The experimental results showed that the rigor binding of a myosin head to actin makes binding of other heads to the same

filament far more favorable than binding to bare filaments [26]. This implies that the binding of one myosin head in ADP/nucleotide-free states induces the increase of the binding affinity of adjacent subunits for ADP/nucleotide-free-myosin. This is not inconsistent with our argument (see Fig. 1b), which is described as follows. The rigor binding of one myosin head induces the conformational changes in the nearby actin subunits, with the changed conformations having higher affinities for myosin in ADP/nucleotide-free states than the unchanged conformation of actin subunits (for simplicity but without influence of our results, in Fig. 1a we draw the same binding affinity E_s for all actin subunits). However, it is noted that ATP–myosin complex has a very different conformation of residues near the actin-binding site from that of ADP/nucleotide-free-myosin. Thus, it is argued that the conformational change of actin subunits induced by rigor binding of myosin should have different or opposite effects on binding affinity of ATP–myosin and that of ADP/nucleotide-free-myosin. Consequently, the changed conformations of actin subunits are supposed to show weaker binding affinities than the unchanged conformation (as shown in Fig. 1b) for ATP–myosin complex.

It is mentioned that, although it had been acknowledged that the strong interaction of myosin with actin results in the structural change to the actin, the role that such structural change would play in actomyosin-based motility remained undefined [25]. As we will show later, it is based on this structure-change-induced reduction of the interaction strength between the myosin motor domain and the local binding sites that myosin-IX moves along the actin with a high mechanochemical coupling efficiency and a high processivity. Moreover, it was based on this structure-change-induced reduction of the interaction we have proposed that the dimeric myosin-VI moves processively in a hand-over-hand running manner [28].

It is interesting to note that, in actin cosedimentation experiments, a subpopulation of ATP–myosin-IX complex binds actin with a remarkably high affinity [19,29,30]. Then it is puzzling that ATP binding to nucleotide-free actomyosin-IX can induce the transition from a strong-binding state to a state that the myosin-IX binds actin weakly enough to allow it to diffuse freely along actin. However, as we will show later, based on the above discussion of the temporal evolution of the binding affinities of several local actin monomers for myosin, the puzzling phenomenon that ATP binding to the nucleotide-free actomyosin-IX can induce the diffusion of myosin-IX along actin can be readily explained. On the other hand, when the preincubated solution of myosin-IX and ATP is mixed with actin, as done in the actin cosedimentation experiments [19,29,30], the ATP–myosin-IX complex has a higher affinity for actin, because the actin has not been deformed by myosin.

2.2. Transition of actin–myosin affinity induces rotation of lever arm

From previous experimental evidence, it is believed that the binding affinity between actin and myosin determines the relative orientation of the lever arm with respect to the motor domain [23,31–37]. This is similar to the case of kinesin–microtubule complexes (see, e.g., Kikkawa [38]). The relative orientation of the lever arm to the motor domain of myosin can be schematically shown in Fig. 2, where Fig. 2a corresponds to the strong-binding state and Fig. 2b to the weak-binding state [39]. In other words, the change from the strong binding (corresponding to closed clefts between the 50 kDa subdomains) to weak binding (corresponding to open clefts between the 50 kDa subdomains) to actin upon ATP binding to myosin leads to the rotation of the lever arm from that as shown in Fig. 2a to that as shown in Fig. 2b; while the change from the weak to strong bindings occurring after ATP hydrolysis but prior to Pi release [40–42] leads to the opposite rotation. This is, the rotation of the lever arm form that as shown in Fig. 2b to that as shown in Fig. 2a occurs with the transition $AM \cdot ADP.Pi \rightarrow AM^* \cdot ADP.Pi$, where A denotes actin, M denotes myosin, $AM \cdot ADP.Pi$ denotes the weak-binding state between actin and myosin and $AM^* \cdot ADP.Pi$ denotes the strong-binding state.

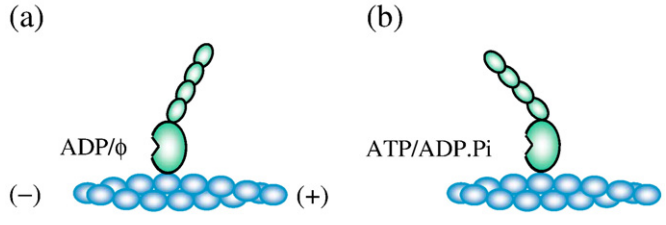

Fig. 2. Orientations of the lever arm relative to the motor domain of myosin-IX with different binding states to actin. (a) Strong-binding state; (b) weak-binding state.

2.3. Mechanism of unidirectional diffusion

Based on the temporal evolution of the binding affinity of actin for myosin (Fig. 1) and the rotations of the lever arm (Fig. 2), we propose a model to describe the processive movement of myosin-IX along actin as shown in Fig. 3.

We begin with the motor domain of myosin-IX being in nucleotide-free rigor state and binding strongly to actin monomer 0, as shown in Fig. 3a. After ATP binding, the binding affinities of the motor domain for its nearby 5 actin monomers become very weak

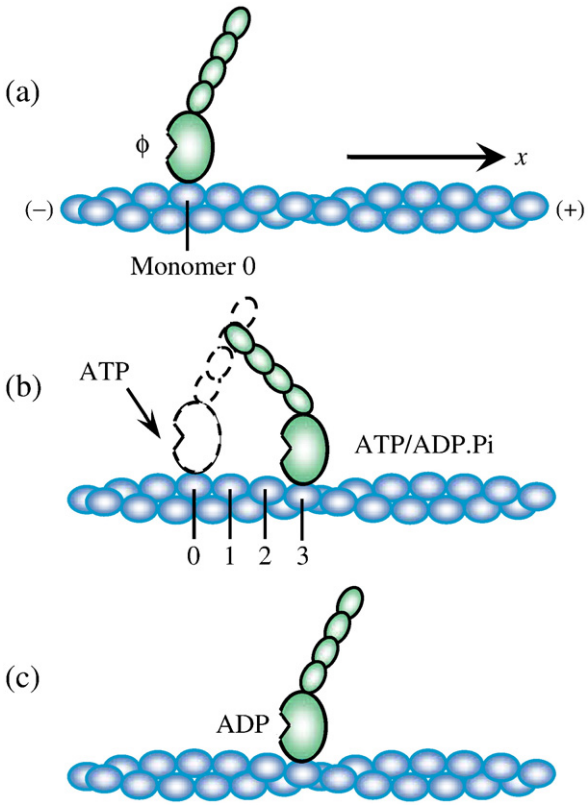

Fig. 3. Schematic illustrations of myosin-IX movement mechanism. (a) Myosin-IX in nucleotide-free state binds strongly to actin monomer 0. (b) After ATP binding, the lever arm rotates in the anti-clockwise direction. During this rotation, a Stokes force is present pointing towards the opposite direction to the rotation, i.e., towards the plus end of actin (or the forward direction). Due to the asymmetry of the potential, myosin-IX has a larger probability to diffuse towards the plus end of actin than towards the minus end. Moreover, the forward Stokes force induced by the rotation of lever arm increases further the probability to diffuse towards the plus end. Once the motor domain diffusing to actin monomer 3 whose conformation has not been affected by the strong interaction with myosin-IX in ADP and nucleotide-free states, the motor domain becomes motionless if the binding affinity E_w is large enough. (c) After ATP hydrolysis but prior to Pi release, the motor domain binds strongly to actin monomer 3 and the lever arm returns to the strong-binding orientation.

(see Fig. 1b) and the lever arm of the myosin-IX starts to rotate in the counter-clockwise direction (see Fig. 2). During this rotation, there exists a Stokes force pointing towards the opposite direction to the rotation, i.e., towards the plus end of actin (or the forward direction). Due to the asymmetric potential, myosin-IX has a larger probability to diffuse towards the plus end of actin than towards the minus end. Moreover, the forward Stokes force induced by the rotation of lever arm increases further the probability to diffuse towards the plus end. Once the motor domain diffusing to actin monomer 3 whose conformation has not been affected by the strong interaction with myosin-IX in ADP and nucleotide-free states, the motor domain becomes motionless if the binding affinity E_w is large enough, as schematically shown in Fig. 3b. After ATP hydrolysis but prior to Pi release, the motor domain becomes bound strongly to actin monomer 3 and then the lever arm rotates in the clockwise direction towards the strong-binding orientation, as shown in Fig. 3c. Note that during this latter rotation there also exists a Stokes force acting on the lever arm, which now points towards the minus end of actin. However, due to the very strong binding of the motor domain to actin, this Stokes force cannot drive the myosin to move along actin anymore. Thus, the motor domain remains fixed at the actin monomer 3. After ADP release, a chemical cycle is finished, and a mechanical step from site 0 to site 3 is made.

The mathematical description of the model is presented in Appendices A and B, where the moving dynamics of myosin-IX during one ATPase cycle is described by Eq. (6a) and (6b) (see Appendix A) and the moving velocity related to kinetic rates and the moving dynamics is given by Eq. (13) (see Appendix B).

3. Results

Eq. (6a) and (6b) (see Appendix A) is solved numerically solved by using stochastic Runge–Kutta algorithm, as used elsewhere [43,44]. For the calculation, we firstly determine values of relevant parameters. To satisfy the requirement of $y \geq y_0$, in the calculation we add a constant term of 3 pN on the right-hand side of Eq. (6b) (see Appendix A) whenever $y < y_0$. At saturating ATP concentration, the time taken in the strong-binding state (with potential $V_s^{(x)}$ shown in Fig. 1a) is $t_s = 100$ ms, which is consistent with the measured ADP-release rate, $k_D \approx 10\ s^{-1}$ [30]. From the observed ATP-turnover rate, $k_c \approx 2\ s^{-1}$ [30], we take the total time in the weak-binding state (with potential $V_w^{(x)}$ shown in Fig. 1b and c) as $t_w = k_c^{-1} - k_D^{-1} = 400$ ms. The time taken in the state with potential $V_w^{(x)}$ shown in Fig. 1b corresponds to the relaxation time t_r, as defined in Fig. 1. It has been known that conformational changes of large biomolecules typically occur on the millisecond time scale. Thus, in the calculation we take $t_r = 2$ ms. Then the time taken in the state with potential $V_w^{(x)}$ shown in Fig. 1c is $t_w - t_r = 398$ ms. Moreover, we have checked that, by taking $t_r = 5$ ms or $t_r = 10$ ms, we obtained the same statistical results. Since the Debye length inside the cell is about 1 nm, we take $a = 1$ nm. As discussed in Fig. 1, E_w should be larger than E_{w2} and E_{w2} should be larger than E_{w1}. Without loss of generality, we take $E_{w1} = \frac{1}{4}E_w$ and $E_{w2} = \frac{1}{2}E_w$ in the calculation, with E_w as an adjustable parameter (see below). We have checked that, by taking other relations of E_{w2}, E_{w2} and E_w, such as $E_{w1} = \frac{1}{3}E_w$ and $E_{w2} = \frac{1}{2}E_w$, we obtained the almost same statistical results. Besides E_w, the asymmetric parameter α of the potential and the rotational time T of the lever arm are also taken as adjustable parameters.

3.1. Motion without external load

First, we study the movement of myosin-IX under no external load. In Fig. 4 we show a typical result for the trace of movement of myosin-IX motor domain at saturating ATP concentration, with $E_w = 13k_BT$, $\alpha = 0.091$ ($d_s = 0.5$ nm) and $T = 10$ μs, where the motor domain is initially ($t = 0$) positioned at $x = 0$ and $y = 0$. In our simulation of

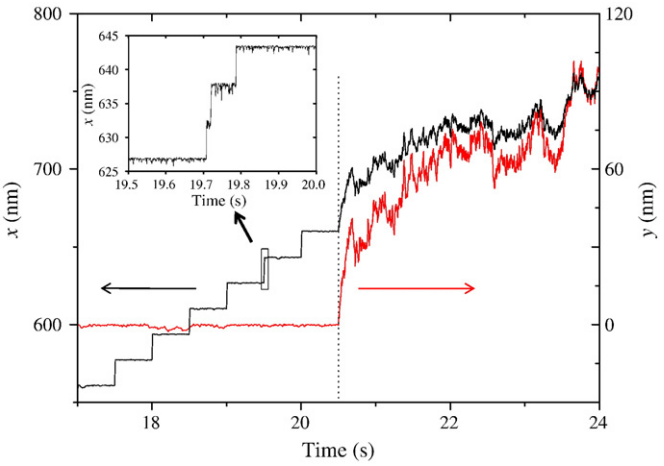

Fig. 4. A typical trace for the motion of myosin-IX motor domain. At $t = 20.5$ s (dotted lines), the myosin is detached from actin and then becomes diffusing freely. Inset is the enlargement of the box region. $E_w = 13k_BT$, $\alpha = 0.091$ ($d_s = 0.5$ nm) and $T = 10$ μs.

Fig. 4, we take the time of the strong-binding state, t_s, and that of the weak-binding state, t_w, to be constant, with $t_s = 100$ ms and $t_w = 400$ ms (see above). It should be noted that either taking t_s and t_w to be constant or taking them to have a distribution but with their mean values equal to the corresponding constant values has no effect on our statistical results presented in this work. The value of $T = 10$ μs taken here is consistent with the available experimental result [33]. For simplicity, the rotation time T, which is related to the Stokes force, is also taken to be constant here. As it is just mentioned for t_s and t_w, either taking T to be constant or taking it to have a distribution but with its mean value equal to the constant value has no effect on the statistical results. To have an intuition on the magnitude of the Stokes force resulting from the rotation of the lever arm, we plot in Fig. S1 (see Appendix C) the Stokes force acting on the motor during the rotation of the lever arm from $\theta(t = 0) = -30°$ to $\theta(t = T) = 50°$ with $T = 10$ μs. Since values of E_w and α are not available experimentally, they are determined by comparing the calculated results with the available experimental data for myosin-IX. As it will be seen below (Figs. 5–9), using values of $E_w = 13k_BT$, $\alpha = 0.091$ ($d_s = 0.5$ nm) and $T = 10$ μs the calculated results are consistent with the experimental data [4]. It is seen from Fig. 4 that, for $t < 20.5$ s, the myosin is bound to actin and moves unidirectionally along actin with a step size of about 16.5 nm. This is consistent with the experiment of Nishikawa et al. [4],

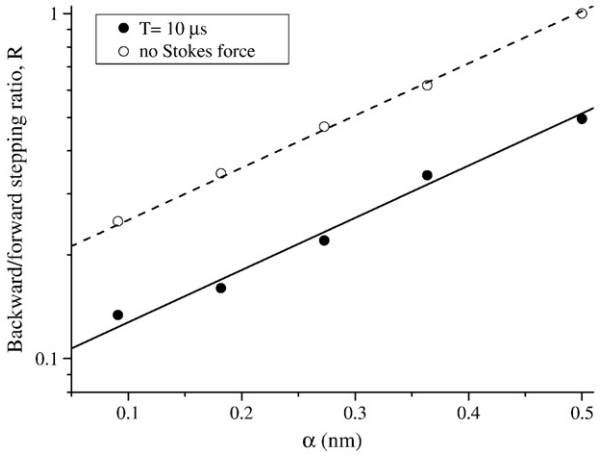

Fig. 5. Backward/forward stepping ratio R versus α with and without considerations of the effect of relative rotation between the neck domain and the motor domain. Lines are fittings by using $R = A_0\exp(\alpha/\alpha_0)$, with $\alpha_0 = 0.287$ for all lines, $A_0 = 0.09$ for $T = 10$ μs while $A_0 = 0.178$ without the Stokes force.

showing that the step sizes are 1.9 ± 4.7 nm and 21 ± 5.6 nm in the presence of 10 and 100 μM ATP, respectively. As seen in the inset of Fig. 4, one step of size of 16.5 nm is actually composed of three substeps of size of 5.5 nm. At $t = 20.5$ s, the myosin is detached from actin and then becomes diffusing freely.

The processive movement of myosin-IX can be characterized by two parameters, the ratio of backward versus forward steps, R, and the dissociation probability, P, per step or per ATPase cycle. The former is related to the mean velocity of the unidirectional movement via $V = Sk(1-R)/(1+R)$ and the latter to the mean run length via $L = S/P$ for $R \ll 1$, where $S = 16.5$ nm is the step size. Parameter k is the ATPase rate, which is dependent on ATP concentration via Michaelis–Menten relation, $k = \frac{k_c[\mathrm{ATP}]}{[\mathrm{ATP}] + k_c / k_b^{(\mathrm{ATP})}}$, where $k_b^{(\mathrm{ATP})}$ is the ATP-binding rate (see Appendix B). It is interesting to study the dependence of these two parameters R and P on E_w and α, which are characteristic of the interaction potential $V_w(x, y)$, and the rotational time T of the neck domain relative to the motor domain. The numerical results showed that R is nearly independent of E_w while is sensitive to α and T. Fig. 5 shows R versus α with $T = 10$ μs and without consideration of the Stokes force, i.e., taking $v_i^{(x)} = v_i^{(y)} = 0$ in Eq. (6a) and (6b) (see Appendix A). The latter case is equivalent to $T \to \infty$. As anticipated, for a given T, R increases as α increases, approximately with a relation of $R = A_0 \exp(\alpha/\alpha_0)$, where $\alpha_0 = 0.287$ is independent of T while A_0 is dependent of T. The forward Stokes force enhances the unidirectional motion and, due to its effect, the myosin-IX can still make a unidirectional movement even at $\alpha = 0.5$ ($d_s = d/2$), at which the motor diffuses directionless if there is no Stokes force. From these results, it is thus concluded that the backward/forward stepping ratio is determined by both the asymmetry of the periodic potential of myosin interacting with actin and the rotational time of the neck domain relative to the motor domain.

In Fig. 6a and Fig. 6b we show, respectively, the mean dissociation probability per step, P, and the mean number of steps versus E_w for different values of α, with $T = 10$ μs and $T \to \infty$ (or without the Stokes force). It is seen that the mean dissociation probability P and the mean number of steps are critically sensitive to E_w, while are nearly independent of α and T. In general, P decreases as E_w increases (Fig. 6a), implying that the mean run length increases as E_w increases (Fig. 6b). Interestingly, it is seen that, for $E_w \leq 6k_BT$, the mean dissociation probability per step is 100% (Fig. 6a), implying that the single-headed myosin is a nonprocessive motor (Fig. 6b). For $E_w > 6k_BT$, the mean dissociation probability per step decreases and thus the mean number of steps increases with the increase of E_w. In particular, for $E_w \geq 11.5k_BT$, the mean dissociation probability per step $P \approx 3.3\%$, implying that myosin-IX can take, on average, nearly about 30 steps before detaching from actin, which is consistent with the experimental data of Nishikawa et al. [4]. From the results shown in Fig. 6, it is thus concluded that the processivity of a single-headed myosin is mainly determined by its binding affinity for actin in ATP state. Some molecules such as the muscle myosin that have a low affinity (e.g., $E_w \leq 6k_BT$) for actin in weak-binding state are non-processive motors; while others such as myosin-IX molecules that have a high affinity (e.g., $E_w \geq 11.5k_BT$) in weak-binding state due to the presence of unique loop 2 insertion are processive motors. The high actin affinity of myosin-IX due to the presence of unique loop 2 is supported by the experiment showed that the deletion of the loop 2 insertion in myosin-IX reduced the actin affinity [30]. Fig. 7 shows a histogram of the number of steps. The histogram can be well fitted by a single-exponential function, which is in good agreement with the experimental data [4].

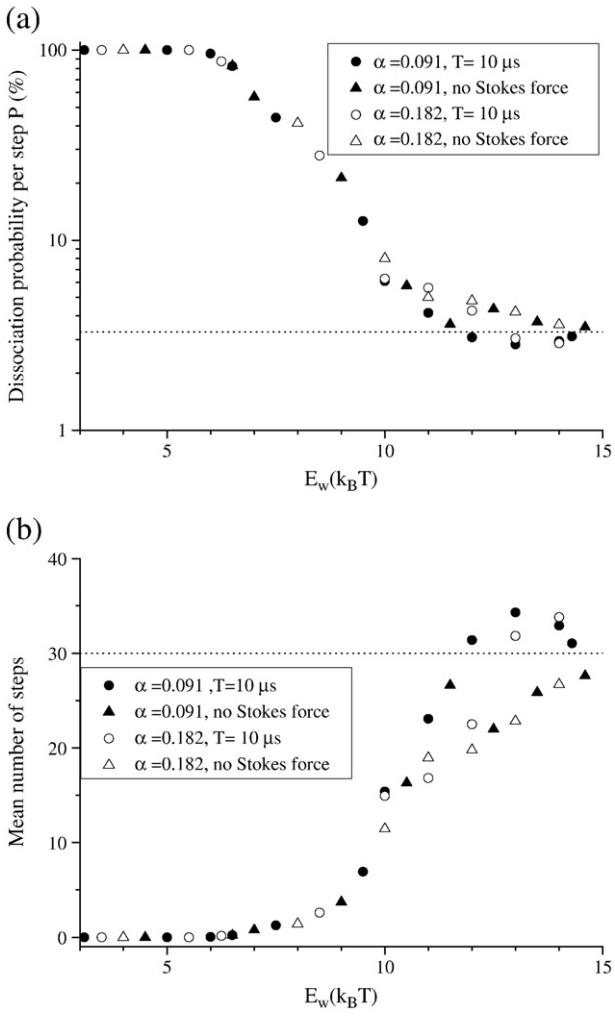

Fig. 6. Processivity versus weak-binding affinity E_w for different values of α, with and without considerations of the effect of relative rotation between neck domain and motor domain. When the motor domain moves away from actin by a vertical distance of 50 nm it is considered that myosin-IX is dissociated from actin. (a) Dissociation probability per step P. The broken line corresponds to $P = 3.3\%$. (b) The mean number of steps calculated from a. The broken line corresponds to 30 steps.

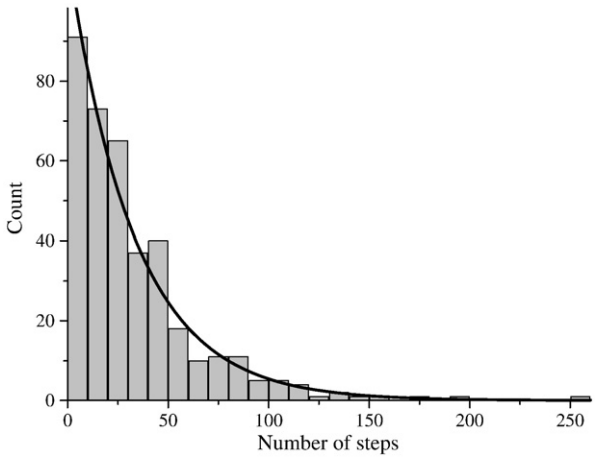

Fig. 7. Histogram of the number of steps calculated with $E_w = 13k_BT$, $\alpha = 0.091$ ($d_s = 0.5$ nm) and $T = 10$ μs. The line is the fitting to the histogram by using $C \cdot \exp(-N/N_0)$, with C being constant and $N_0 = 33$.

3.2. Motion with external load

Now we study the movement of myosin-IX under the external load, F_{load}, which is defined as positive when it is pointed backwards. To this end, we simply add a term $-F_{\mathrm{load}}$ on the right-hand side of

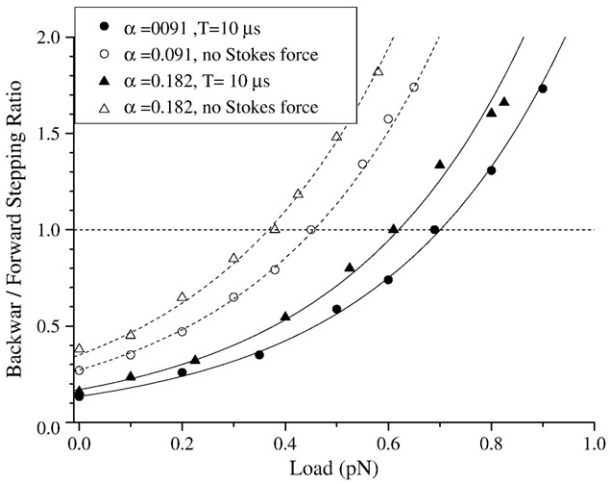

Fig. 8. Backward/forward stepping ratio R versus backward load F_{load} for different values of α, with and without considerations of the effect of relative rotation between the neck domain and the motor domain. $E_w = 13k_BT$. Lines are fittings by using $R = R_0\exp(F_{load}/F_0)$, with $F_0 = 0.35$ pN for all lines, $R_0 = 0.135$ for $\alpha = 0.091$ and $T = 10$ μs, $R_0 = 0.17$ for $\alpha = 0.182$ and $T = 10$ μs, $R_0 = 0.272$ for $\alpha = 0.091$ and no Stokes force, and $R_0 = 0.35$ for $\alpha = 0.182$ and no Stokes force.

Eq. (6a) (see Appendix A). In Fig. 8 we show R versus F_{load} for different values of α with consideration of Stokes force (with $T = 10$ μs) and without consideration of Stokes force (with $T \to \infty$). First, we note that, for a fixed set of α and T, R increases exponentially with the increase of F_{load}, i.e., $R = R_0\exp(F_{load}/F_0)$, where $F_0 = 0.35$ pN is independent of α and T while R_0 is the ratio of backward versus forward steps under zero external load, dependent of α and T (see also Fig. 5). This relation of R versus F_{load} satisfies Arrhenius equation. Second, it is seen that, the Stokes force with $T = 10$ μs can enhance the mean stall force, F_{stall}, at which the ratio R becomes equal to 1, by about 0.24 pN (or by about 55%).

In Fig. 9 we show the mean stall force F_{stall} versus T for different values of α. It is seen that, when T is larger than 200 μs, the rotation of the neck domain has no influence on the movement of myosin-IX; when $T \le 100$ μs, the mean stall force increases with the decrease of T; and when $T \le 10$ μs, the mean stall force increases almost linearly with the decrease of $\log(T)$. As expected, when $\alpha = 0.5$ ($d_s = d/2$) the mean stall force is zero in the absence of Stokes force (with $T \to \infty$). For a given T, the mean stall force decreases with the increase of α. For example, when α decreases from 0.5 ($d_s = d/2$) to 0.091 ($d_s = 0.5$ nm), the mean stall force increases by about 0.45 pN for a given T.

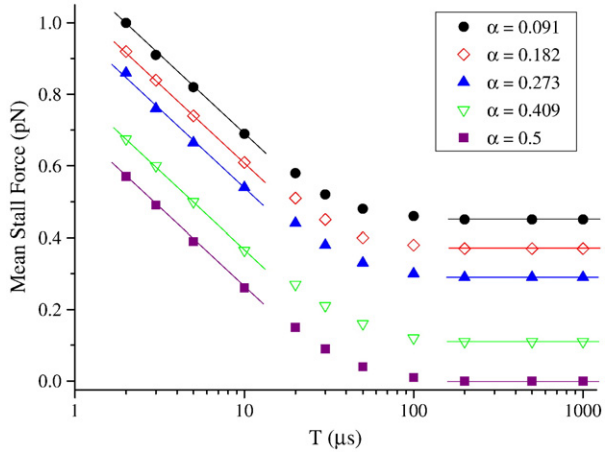

Fig. 9. Mean stall force F_{stall} versus rotational time T of the neck domain relative to the motor domain for different values of α. $E_w = 13k_BT$.

From these results (Figs. 8 and 9), it is thus concluded that, as the backward/forward stepping ratio, the mean stall force of myosin-IX is also determined by both the asymmetry of the periodic potential of myosin interacting with actin and the rotational time of the neck domain relative to the motor domain. In particular, from Fig. 9 it is noted that, for $\alpha = 0.091$ ($d_s = 0.5$ nm), when $T \le 10$ μs the mean stall force $F_{stall} \ge 0.7$ pN, which is consistent with the experimental data (see Fig. 1A of Nishikawa et al. [4]).

In one word, from Figs. 4–9 it is noted that, by taking $\alpha = 0.091$ ($d_s = 0.5$ nm), $E_w \ge 11.5k_BT$ and $T = 10$ μs, our model gives the results such as the step size per ATPase cycle, the large forward/backward stepping ratio, the mean run length and the mean stall force that are in agreement with the experimental data for myosin-IX.

3.3. Kinetics

It is noted from our results (see, e.g., Fig. 4) that, during one step, the moving time is very short (shorter than 1 ms), which is much shorter than the dwell time. Thus, it is a good approximation that the dwell time in one step is equal to the time taken by one step. From Eq. (10) (see Appendix B), it is seen that, at low ATP concentration, which implies $k_1 \ll k_2$, k_3, k_4, the dwell time distribution is approximately single exponential, i.e., $f(t) \approx k_1\exp(-k_1t)$, with $k_1 = k_b^{(ATP)}[ATP]$. This is consistent with the experimental data for human myosin-IX [4].

At saturating ATP concentration, which implies k_2, k_3, $k_4 \ll k_1$, the form of the dwell time distribution is determined by the relative values among k_2, k_3 and k_4, which is written from Eq. (10) (see Appendix B) as

$$f(t) \approx k_2k_3k_4\left\{\frac{e^{-k_2t}}{(k_3-k_2)(k_4-k_2)} + \frac{e^{-k_3t}}{(k_2-k_3)(k_4-k_3)} + \frac{e^{-k_4t}}{(k_2-k_4)(k_3-k_4)}\right\}.$$

From the experiment for rat myosin-IX by Nalavadi et al. [30], we have $k_c = k_2k_3k_4/(k_2k_3 + k_2k_4 + k_3k_4) \approx 2\ s^{-1}$ and $k_4 \approx 10\ s^{-1}$, implying $k_2k_3/(k_2 + k_3) \approx 2.5\ s^{-1}$. The dwell time distribution for $k_4 = 10\ s^{-1}$ and different values of k_2 and k_3 are shown in Fig. 10. It is seen that, for any choice of values of k_2 and k_3, the distribution has the maximum at an intermediate value of t. This will give that the velocity distribution has the maximum at an intermediate value of the velocity, which is consistent with the experimental data [4].

4. Discussion

In this work, a new Brownian ratchet model is presented for the processive movement of single-headed myosin-IX along actin. An important point in the model is that the conformational changes in several local actin monomers induced by the strong binding of rigor myosin play an active role in the motility of single-headed myosin-IX, in contrast to the common belief that the actin acts only as a passive track for the motility of myosin. Moreover, the effect of Stokes force resulting from the rotation of the neck domain relative to the motor domain on the motility is also considered in the model, which shows that it can enhance the unidirectional movement of myosin-IX. One of important conclusions from the model is that the processivity of a single-headed myosin is mainly determined by its binding affinity for actin in ATP state (see Fig. 6). This provides a good explanation to the high processivity of myosin-IX, which results from its high binding affinity for actin in ATP state due to the presence of unique loop 2 insertion or N-terminal extension [30]. It is noted that, in actin cosedimentation experiments, a subpopulation of ATP–myosin-IX complex bound actin with a high affinity and another subpopulation did not bind actin [30], implying a low binding affinity. Interestingly, in the single-molecule experiments, two forms of myosin-IX existed, with one having processive motility and the other one having

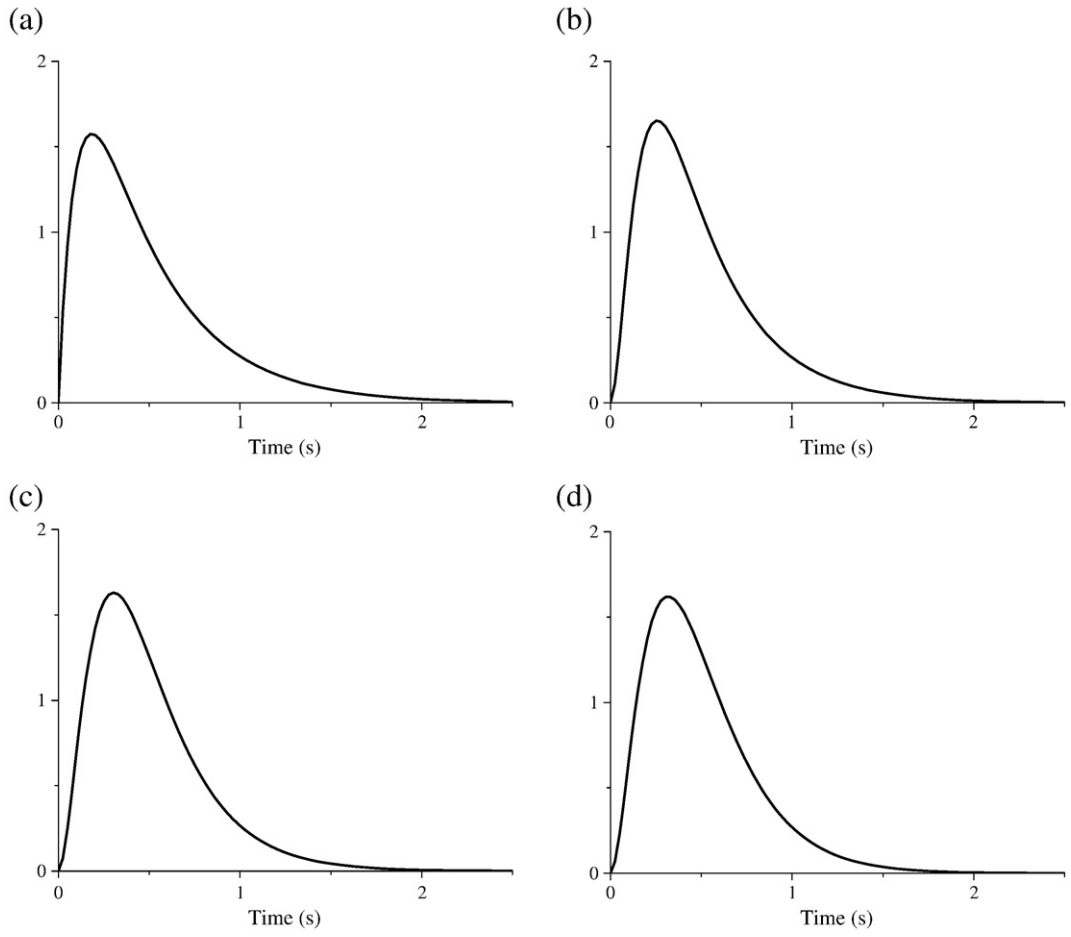

Fig. 10. Dwell time distribution with $k_4 = 10\ s^{-1}$ and (a) $(k_2,k_3) = (\infty, 2.5\ s^{-1})$ or $(2.5\ s^{-1}, \infty)$, (b) $(k_2,k_3) = (15\ s^{-1}, 3\ s^{-1})$ or $(3\ s^{-1}, 15\ s^{-1})$, (c) $(k_2,k_3) = (7.5\ s^{-1}, 3.75\ s^{-1})$ or $(3.75\ s^{-1}, 7.5\ s^{-1})$, and (d) $(k_2,k_3) = (5.625\ s^{-1}, 4.5\ s^{-1})$ or $(4.5\ s^{-1}, 5.625\ s^{-1})$.

nonprocessive motility [4]. These results are exactly consistent with our conclusion that the subpopulation of ATP–myosin-IX complex that bind actin with a high affinity have processive motility while the other subpopulation that bind actin with a low affinity have nonprocessive motility.

The present model is different, in many aspects, from the conventional Brownian ratchet model presented in the literature [16–18]. First, in the conventional model the nucleotide transition induces the fluctuation of the actin–myosin interaction potential at any spatial position along the actin (i.e., the global potential); whereas in the present model the nucleotide transition induces fluctuations of both the global potential and the actin–myosin interaction potential only at spatial positions near which the myosin is positioned (i.e., the local potential). The fluctuation of the global potential results from the conformational change of the myosin, while the change of the local potential results from the conformational change of the actin monomers near which the myosin is bound to, which is in turn caused by its strong interaction with the myosin in rigor state. The fluctuation of the global potential in the conventional model gives a Markov process, while the fluctuation of the local potential in the present model gives a non-Markov process. This argument of the local potential is somewhat similar to that of the potential slope due to conformational changes in the actin filament, as proposed by other researchers (see, e.g., Okada et al. [45]). Second, in the conventional model there exists no directed "driving force" and the fluctuation of the asymmetric periodic potential produces the unidirectional movement of the motor; while in the present model both the fluctuation of the asymmetric periodic potential and the directed "driving force" contribute to the unidirectional movement, and even for the symmetric periodic potential the motor can still make the unidirectional movement due to the presence of the directed "driving force." Third, in the conventional model, in order to have a net unidirectional movement, it is required that the potential depth in weak-binding state should be very shallow, which leads to a very low processivity or no processivity; while in the present model the potential depth in weak-binding state is not shallow, which gives a high processivity.

It was reported that native myosin-IX is a plus-end-directed molecular motor [3]. However, the construct of myosin-IX by removal of the tail domain was reported to move towards the minus end of actin [2]. Based on the present model, this may be understood as follows. As suggested by O'Connell and Mooseker [3], the tail domain may interact with the motor domain, which induces the conformational change in the residues near the actin-binding site of the motor domain. This conformational change induces the redistribution of the charge, resulting in the change in the asymmetry of the interaction potential between the motor domain and the actin. Due to the interaction between the motor domain and tail, the interaction potential between the motor domain and actin has a small value of α, and thus myosin moves processively towards the plus end; while without the interaction between head and tail, the interaction potential is changed to a large α that is close to 1. It is verified that, when $\alpha > 0.691$, the myosin-IX becomes moving backwards processively even with $T = 10\ \mu s$ (see Fig. 11).

The argument of the difference of the local interaction potential from the potential elsewhere between myosin and actin adopted here is similar to that adopted for the interaction between kinesin and the microtubule [43,44]. In the latter case, the change of the local

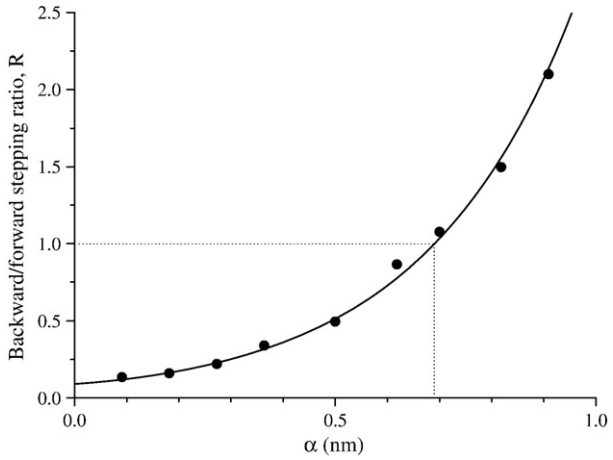

Fig. 11. Backward/forward stepping ratio R versus α by including the effect of relative rotation between the neck domain and the motor domain, with $T=10$ μs. The line is the fitting by using $R=A_0\exp(\alpha/\alpha_0)$, with $\alpha_0=0.287$ and $A_0=0.09$.

potential also results from the conformational change of the microtubule α and β heterodimer unit, which is in turn caused by its strong interaction with the kinesin in rigor state. As in the case of myosin-IX, where the high actin affinity of myosin-IX in the weak-binding state (or ATP state) due to the presence of unique loop 2 [19,29,30] ensures the processive movement of myosin-IX, the high affinity of single-headed kinesin such as KIF1A in the weak-microtubule-binding state (or ADP state) due to the presence of the K loop [46,47] ensures the high processivity of KIF1A [43]. Moreover, based on the structure-change-induced reduction of the interaction between myosin and actin it has been proposed that the dimeric myosin-VI can move processively in a hand-over-hand running manner [28]. Therefore, the local structural changes in the track induced by the strong binding of motor proteins in rigor state may generally play an important role to the motility of the motor proteins. In addition, it is noted that the present model may also be implicated in the multiple steps (e.g., see the inset of Fig. 4) of muscle myosin per ATP hydrolysis observed by Yanagida and his colleagues [48] and of single-headed myosin-V per ATP hydrolysis observed by Okada et al. [45].

It is noted that throughout our calculations in this work we have taken the same viscous drag both on the motor domain and on the lever arm of myosin-IX. In a more realistic situation, it is expected that a higher viscous drag on the motor domain, which is sliding in close proximity of the actin filament, than on the lever arm. To see this effect on the moving dynamics, we take the viscosity around the motor domain equal to 2-fold of that (the viscosity of solution) around the lever arm, i.e., take $\Gamma=2\Gamma_i r/r_L$ and keep Γ_i unchanged in Eq. (6a) and (6b). The numerical results show that, although this has an obvious effect on the moving time during one step (i.e., the time for the motor domain to move from subunit 0 to subunits ±3), it only has a very slight effect on the forward/backward stepping ratio and on the mean stall force: for example, for $E_w=13k_BT$, $\alpha=0.091$ and $T=10$ μs, the moving time is increased by about 20%, but either the forward/backward stepping ratio or the mean stall force is changed by a magnitude smaller than 2%. However, it is noted from Eq. (6a) that, if Γ_i is increased, which induces the increase of the "driving force," i.e., the first term in the right-hand side of Eq. (6a), this results in the increase of both the forward/backward stepping ratio and the stall force.

Finally, it is noted that an important prediction of the present model is that the prosessivity of myosin-IX decreases with the decrease of its binding affinity for actin in ATP state. To test this prediction, one can make mutations to the actin-binding residues of myosin-IX and measure the mean run length versus the binding affinity (or the equilibrium dissociation constant) of these mutant myosin-IX molecules in complex with non-hydrolysable ATP analogues for (or from) actin, thus comparing with the corresponding theoretical results (Fig. 6b). Moreover, our results predict that, without the effect of the Stokes force, the ratio of backward versus forward steps is increased (see Fig. 5) and the stall force is decreased (see Figs. 8 and 9). Thus, it is interesting to experimentally measure the backward/forward stepping ratio and the stall force of the mutant myosin-IX by deletion of some IQ motifs in the neck domain and compare the measured values of mutant myosin-IX with those of the wild type.

Acknowledgment

This work is supported by the National Natural Science Foundation of China (grant no. 10974248).

Appendix A. Equations for moving dynamics of myosin-IX

Based on the present model (Fig. 3), we give a simplified quantitative analysis to the dynamics of myosin-IX. The motor domain is approximated as a sphere with a radius $r=5$ nm. The lever arm of length $l_L\approx20$ nm consists of four IQ domains and each IQ domain is approximated as a sphere with radius $r_L=2.5$ nm. During the rotation of the lever arm, as shown in Fig. 3b, the coordinates of the motor domain (x and y) relative to those of the ith sphere (x_i and y_i) of the lever arm are written as follows

$$\frac{dx_i}{dt}=\frac{dx}{dt}-v_i^{(x)}, \tag{1a}$$

$$\frac{dy_i}{dt}=\frac{dy}{dt}-v_i^{(y)}, \tag{1b}$$

where

$$v_i^{(x)}\approx[2(i-1)+1]r_L\omega\cos\theta, \tag{2a}$$

$$v_i^{(x)}\approx[2(i-1)+1]r_L\omega\sin\theta,\ (i=1,2,3,4) \tag{2b}$$

with ω being the rotational velocity of the lever arm relative to the motor domain. According to the available structures [39], we approximately have θ changing from $\theta(t=0)=-30°$ to $\theta(t=T)=50°$, where T is the rotational time. For simplicity, considering that the rotational velocity is time independent during the rotation we have $\omega=80°/T$ and $\theta(t)=-30^\circ+\frac{80^\circ}{T}t$. From the experimental results [33], T is in the order of ten times of microsecond. The Stokes force acting on the ith sphere is obtained as

$$F_i^{(x)}=-\Gamma_i\frac{dx_i}{dt}, \tag{3a}$$

$$F_i^{(y)}=-\Gamma_i\frac{dy_i}{dt}, \tag{3b}$$

where the Stokes coefficient Γ_i is approximated as $\Gamma_i=6\pi\eta r_L$, with the viscosity of the aqueous medium $\eta=0.015$ g cm^{-1} s^{-1} [49]. From Eqs. (1a) and (1b) and (3a) and (3b) we have

$$F_i^{(x)}=-\Gamma_i\frac{dx}{dt}+\Gamma_i v_i^{(x)}, \tag{4a}$$

$$F_i^{(y)}=-\Gamma_i\frac{dy}{dt}+\Gamma_i v_i^{(y)}. \tag{4b}$$

The movement of the motor domain during the stepping period can be described by the following Langevin equation

$$\Gamma\frac{dx}{dt} = \sum_i F_i^{(x)} - \frac{\partial}{\partial x}V_w(x,y,t) + f_x(t), \tag{5a}$$

$$\Gamma\frac{dy}{dt} = \sum_i F_i^{(y)} - \frac{\partial}{\partial y}V_w(x,y,t) + f_y(t), \tag{5b}$$

where the drag coefficient on the motor domain $\Gamma = 6\pi\eta r$, $V_w(x, y, t)$ is the weak interaction potential of myosin-IX with actin after ATP binding and then hydrolysis to ADP.Pi (Fig.1b and c), and $f_m(t)$ $(m = x, y)$ is the Gaussian white noise with $\langle f_m(t)\rangle = 0$ and $\langle f_m(t) f_n(t')\rangle = 2k_BT\cdot(\Gamma + \sum_i \Gamma_i)\cdot\delta_{mn}\cdot\delta(t - t')$. Using Eq. (4a) and (4b) we rewrite Eq. (5a) and (5b) as follows

$$\left(\Gamma + \sum_i \Gamma_i\right)\frac{dx}{dt} = \sum_i \Gamma_i v_i^{(x)} - \frac{\partial}{\partial x}V_w(x,y,t) + f_x(t), \tag{6a}$$

$$\left(\Gamma + \sum_i \Gamma_i\right)\frac{dy}{dt} = \sum_i \Gamma_i v_i^{(y)} - \frac{\partial}{\partial y}V_w(x,y,t) + f_y(t). \tag{6b}$$

Note that $v_i^{(x)}$ and $v_i^{(y)}$ are described by Eq. (2a) and (2b) when $t \le T$, while $v_i^{(x)} = v_i^{(y)} = 0$ when $t > T$.

During the dwell period, i.e., in ADP and nucleotide-free states, the motion of myosin is described by the similar equations to those in Eq. (6a) and (6b) but with $V_s(x, y)$ (Fig. 1a) instead of $V_w(x, y, t)$. However, because E_s is very large we have $dx/dt \approx 0$ and $dy/dt \approx 0$, i.e., the motor domain is motionless although the lever arm rotates inversely from 50° to −30°.

Appendix B. Equations for kinetics of myosin-IX

During processive movement, the ATPase cycling pathway of myosin-IX in one step is described by the following scheme

$$(\mathrm{AM})_i \underset{k_{-1}}{\overset{k_1}{\rightleftharpoons}} \mathrm{AM.ATP} \underset{k_{-2}}{\overset{k_2}{\rightleftharpoons}} \mathrm{AM.ADP.Pi} \underset{k_{-3}}{\overset{k_3}{\rightleftharpoons}} \mathrm{AM.ADP} \underset{k_{-4}}{\overset{k_4}{\rightleftharpoons}} (\mathrm{AM})_f, \tag{7}$$

where $(\mathrm{AM})_i$ denotes the initial nucleotide-free actin–myosin-IX complex resulting from the previous step and $(\mathrm{AM})_f$ denotes the final nucleotide-free actin–myosin-IX complex resulting from ADP release in the present step. $k_1 = k_b^{(\mathrm{ATP})}[\mathrm{ATP}]$, with $k_b^{(\mathrm{ATP})}$ denoting ATP-binding rate, $k_{-3} = k_b^{(\mathrm{Pi})}[\mathrm{Pi}]$, with $k_b^{(\mathrm{Pi})}$ denoting Pi-binding rate, and $k_{-4} = k_b^{(\mathrm{ADP})}[\mathrm{ADP}]$, with $k_b^{(\mathrm{ADP})}$ denoting ADP-binding rate. Note that Scheme (7) represents only the minimal pathway because there may exist multiple intermediate states in each of AM.ATP, AM.ADP.Pi and AM.ADP states. In the case of $[\mathrm{ADP}] = [\mathrm{Pi}] = 0$ and considering that $k_{-1} \ll k_1$ at the ATP concentration that is not very low and $k_{-2} \ll k_2$, the ATPase cycling pathway, Scheme (7), can be rewritten as follows

$$(\mathrm{AM})_i \xrightarrow{k_1} \mathrm{AM.ATP} \xrightarrow{k_2} \mathrm{AM.ADP.Pi} \xrightarrow{k_3} \mathrm{AM.ADP} \xrightarrow{k_4} (\mathrm{AM})_f. \tag{8}$$

In the following, we denote the probabilities for finding the actin–myosin-IX complex in $(\mathrm{AM})_i$, AM.ATP, AM.ADP.Pi, AM.ADP and $(\mathrm{AM})_f$ states by ϕ_i, T, DP, D and ϕ_f, respectively. From Scheme (8), the probabilities are described by the following equations

$$\frac{d\phi_i}{dt} = -k_1\phi_i, \tag{9a}$$

$$\frac{dT}{dt} = k_1\phi_1 - k_2T, \tag{9b}$$

$$\frac{d(\mathrm{DP})}{dt} = k_2T - k_3(\mathrm{DP}), \tag{9c}$$

$$\frac{dD}{dt} = k_3(\mathrm{DP}) - k_4D, \tag{9d}$$

$$\frac{d\phi_f}{dt} = k_4D. \tag{9e}$$

By solving Eqs. (9a)–(9e), with the initial conditions at $t = 0$: $\phi_i(0) = 1$, $T(0) = 0$, $DP(0) = 0$, $D(0) = 0$ and $\phi_f(0) = 0$, we obtain the probability density for the time taken by one step, $f(t) = d\phi_f/dt$, as follows

$$f(t) = k_1k_2k_3k_4\left\{\frac{e^{-k_1t}}{(k_2-k_1)(k_3-k_1)(k_4-k_1)} + \frac{e^{-k_2t}}{(k_1-k_2)(k_3-k_2)(k_4-k_2)} + \frac{e^{-k_3t}}{(k_1-k_3)(k_2-k_3)(k_4-k_3)} + \frac{e^{-k_4t}}{(k_1-k_4)(k_2-k_4)(k_3-k_4)}\right\}. \tag{10}$$

From Eq. (10), the mean time taken by one step is

$$T_d = \frac{1}{k_1} + \frac{1}{k_2} + \frac{1}{k_3} + \frac{1}{k_4}. \tag{11}$$

Thus, the mean ATPase rate $k \equiv 1/T_d$ is obtained from Eq. (11) as follows

$$k = \frac{k_c[\mathrm{ATP}]}{[\mathrm{ATP}] + k_c/k_b^{(\mathrm{ATP})}}, \tag{12}$$

where $k_c = k_2k_3k_4/(k_2k_3 + k_2k_4 + k_3k_4)$ is the ATP-turnover rate.

Denoting the ratio of backward versus forward steps as R and the step size as S, the mean velocity of the unidirectional movement of myosin-IX is

$$V = \frac{(1-R)}{(1+R)}kS. \tag{13}$$

Appendix C. Supplementary data

Supplementary data associated with this article can be found, in the online version, at doi:10.1016/j.bpc.2010.05.007.

References

[1] P.L. Post, M.J. Tyska, C.B. O'Connell, K. Johung, A. Hayward, M.S. Mooseker, Myosin-IXb is a single-headed and processive motor, J. Biol. Chem. 277 (2002) 11,679–11,683.
[2] A. Inoue, J. Saito, R. Ikebe, M. Ikebe, Myosin IXb is a single-headed minus-end-directed processive motor, Nat. Cell Biol. 4 (2002) 302–306.
[3] C.B. O'Connell, M.S. Mooseker, Native myosin-IXb is a plus-, not a minus-end-directed motor, Nat. Cell Biol. 5 (2003) 171–172.
[4] M. Nishikawa, S. Nishikawa, A. Inoue, A.H. Iwane, T. Yanagida, M. Ikebe, A unique mechanism for the processive movement of single-headed myosin-IX, Biochem. Biophys. Res. Commun. 343 (2006) 1159–1164.
[5] A.D. Mehta, R.S. Rock, M. Rief, J.A. Spudich, M.S. Mooseker, R.E. Cheney, Myosin-V is a processive actin-based motor, Nature 400 (1999) 590–593.
[6] M. Rief, R.S. Rock, A.D. Mehta, M.S. Mooseker, R.E. Cheney, J.A. Spudich, Myosin-V stepping kinetics: a molecular model for processivity, Proc. Natl. Acad. Sci. U.S.A. 97 (2000) 9482–9486.
[7] A. Yildiz, J.N. Forkey, S.A. McKinney, T. Ha, Y.E. Goldman, P.R. Selvin, Myosin V walks hand-over-hand: single fluorophore imaging with 1.5-nm localization, Science 300 (2003) 2061–2065.
[8] C. Veigel, F. Wang, M.L. Bartoo, J.R. Sellers, J.E. Molloy, The gated gait of the processive molecular motor, myosin V, Nat. Cell Biol. 4 (2002) 59–65.
[9] J.E. Baker, E.B. Krementsova, G.G. Kennedy, A. Armstrong, K.M. Trybus, D.M. Warshaw, Myosin V processivity: multiple kinetic pathways for head-to-head coordination, Proc. Natl. Acad. Sci. U.S.A. 101 (2004) 5542–5546.
[10] S. Uemura, H. Higuchi, A.O. Olivares, E.M. De La Cruz, S. Ishiwata, Mechanochemical coupling of two substeps in a single myosin V motor, Nat. Struct. Mol. Biol. 11 (2004) 877–883.

[11] S.S. Rosenfeld, H.L. Sweeney, A model of myosin V processivity, J. Biol. Chem. 279 (2004) 40,100–40,111.
[12] J.A. Spudich, R.S. Rock, A crossbridge too far, Nat. Cell Biol. 4 (2002) E8–E10.
[13] G. Lan, S.X. Sun, Dynamics of myosin-V processivity, Biophys. J. 88 (2005) 999–1008.
[14] A. Vilfan, Elastic lever arm model for myosin V, Biophys. J. 88 (2005) 3792–3805.
[15] P. Xie, S.-X. Dou, P.-Y. Wang, Model for kinetics of myosin-V molecular motors, Biophys. Chem. 120 (2006) 225–236.
[16] R.D. Astumian, M. Bier, Fluctuation driven ratchets: molecular motors, Phys. Rev. Lett. 72 (1994) 1766–1769.
[17] F. Jülicher, A. Ajdari, J. Prost, Modeling molecular motors, Rev. Mod. Phys. 69 (1997) 1269–1281.
[18] Y. Okada, H. Higuchi, N. Hirokawa, Processivity of the single-headed kinesin KIF1A through biased binding to tubulin, Nature 424 (2003) 574–577.
[19] T. Kambara, M. Ikebe, A unique ATP hydrolysis mechanism of single-headed processive myosin, myosin IX, J. Biol. Chem. 281 (2006) 4949–4957.
[20] M. Iwaki, A.H. Iwane, M. Ikebe, T. Yanagida, Biased Brownian motion mechanism for processivity and directionality of single-headed myosin-VI, Biosystems 93 (2008) 39–47.
[21] M.A. Geeves, K.C. Holmes, Structural mechanism of muscle contraction, Annu. Rev. Biochem. 68 (1999) 687–728.
[22] S. Highsmith, Lever arm model of force generation by actin–myosin–ATP, Biochemistry 38 (1999) 9791–9797.
[23] A. Houdusse, H.L. Sweeney, Myosin motors: missing structures and hidden springs, Curr. Opin. Struct. Biol. 11 (2001) 182–194.
[24] J.A. Spudich, The myosin swinging cross-bridge model, Nat. Rev. Mol. Cell Biol. 2 (2001) 387–392.
[25] M.A. Geeves, R. Fedorov, D.J. Manstein, Molecular mechanism of actomyosin-based motility, Cell. Mol. Life Sci. 62 (2005) 1462–1477.
[26] A. Orlova, E.H. Egelman, Cooperative rigor binding of myosin to actin is a function of F-actin structure, J. Mol. Biol. 265 (1997) 469–474.
[27] E. Prochniewicz, T.F. Walseth, D.D. Thomas, Structural dynamics of actin during active interaction with myosin: different effects of weakly and strongly bound myosin heads, Biochemistry 43 (2004) 10,642–10,652.
[28] P. Xie, S.-X. Dou, P.-Y. Wang, A hand-over-hand diffusing model for myosin-VI molecular motors, Biophys. Chem. 122 (2006) 90–100.
[29] P.L. Post, G.M. Bokoch, M.S. Mooseker, Human myosin-IXb is a mechanochemically active motor and a GAP for rho, J. Cell Sci. 111 (1998) 941–950.
[30] V. Nalavadi, M. Nyitrai, C. Bertolini, N. Adamek, M.A. Geeves, M. Bahler, Kinetic mechanism of myosin IXB and the contributions of two class IX-specific regions, J. Biol. Chem. 280 (2005) 38,957–38,968.
[31] Y.E. Goldman, Wag the tail: structural dynamics of actomyosin, Cell 93 (1998) 1–4.
[32] A. Ishijima, H. Kojima, T. Funatsu, M. Tokunaga, H. Higuchi, H. Tanaka, T. Yanagida, Simultaneous observation of individual ATPase and mechanical events by a single myosin molecule during interaction with actin, Cell 92 (1998) 161–171.
[33] O. Roopnarine, A.G. Szent-Györgyi, D.D. Thomas, Microsecond rotational dynamics of spin-labeled myosin regulatory light chain induced by relaxation and contraction of scallop muscle, Biochemistry 37 (1998) 14,428–14,436.
[34] I. Brust-Mascher, L.E.W. LaConte, J.E. Baker, D.D. Thomas, Myosin light-chain domain rotates upon muscle activation but not ATP hydrolysis, Biochemistry 38 (1999) 12,607–12,613.
[35] N. Volkman, D. Hanein, Actomyosin: law and order in motility, Curr. Opin. Cell Biol. 12 (2000) 26–34.
[36] N. Volkmann, D. Hanein, G. Ouyang, K.M. Trybus, D.J. DeRosier, S. Lowey, Evidence for cleft closure in actomyosin upon ADP release, Nat. Struct. Biol. 7 (2000) 1147–1155.
[37] D.M. Himmel, S. Gourinath, L. Reshetnikova, Y. Shen, A.G. Szent-Gyorgyi, C. Cohen, Crystallographic findings on the internally uncoupled and near-rigor states of myosin: further insights into the mechanics of the motor, Proc. Natl. Acad. Sci. U.S.A. 99 (2002) 12,645–12,650.
[38] M. Kikkawa, The role of microtubules in processive kinesin movement, Trends Cell Biol. 18 (2008) 128–135.
[39] S. Burgess, M. Walker, F. Wang, J.R. Sellers, H.D. White, P.J. Knight, J. Trinick, The prepower stroke conformation of myosin V, J. Cell Biol. 159 (2002) 983–991.
[40] D.A. Smith, J. Sleep, Mechanokinetics of rapid tension recovery in muscle: the myosin working stroke is followed by a slower release of phosphate, Biophys. J. 87 (2004) 442–456.
[41] Y. Takagi, H. Shuman, Y.E. Goldman, Coupling between phosphate release and force generation in muscle actomyosin, Philos. Trans. R. Soc. Lond. B Biol. Sci. 359 (2004) 1913–1920.
[42] M. Sun, M.B. Rose, S.K. Ananthanarayanan, D.J. Jacobs, M. Yengo CM, Characterization of the pre-force-generation state in the actomyosin cross-bridge cycle, Proc. Natl. Acad. Sci. U.S.A. 105 (2008) 8631–8636.
[43] P. Xie, S.-X. Dou, P.-Y. Wang, Processivity of single-headed kinesin motors, Biochim. Biophys. Acta 1767 (2007) 1418–1427.
[44] P. Xie, Stepping behavior of two-headed kinesin motors, Biochim. Biophys. Acta 1777 (2008) 1195–1202.
[45] T. Okada, H. Tanaka, A.H. Iwane, K. Kitamura, M. Ikebe, T. Yanagida, The diffusive search mechanism of processive myosin class-V motor involves directional steps along actin subunits, Biochem. Biophys. Res. Commun. 354 (2007) 379–384.
[46] Kikkawa M, Okada Y, Hirokawa N, 2000. 15 Å resolution model of the monomeric kinesin motor, KIF1A. Cell 100 (2000) 241–252.
[47] Nitta R, Kikkawa M, Okada Y, Hirokawa N, 2004. KIF1A alternately uses two loops to bind microtubules. Science 305 (2004) 678–683.
[48] K. Kitamura, M. Tokunaga, A.H. Iwane, T. Yanagida, A single myosin head moves along an actin filament with regular steps of 5.3 nanometres, Nature 397 (1999) 129–134.
[49] R. Swaminathan, C.P. Hoang, A.S. Verkman, Photobleaching recovery and anisotropy decay of green fluorescent protein GFP-S65T in solution and cells: cytoplasmic viscosity probed by green fluorescent protein translational and rotational diffusion, Biophys. J. 72 (1997) 1900–1907.